

Hybrid Silicon Evanescent Phase Modulator Based on Carrier Depletion in Offset Multiple-Quantum-Well

Hui-wen Chen, Ying-hao Kuo, and John E. Bowers

Department of Electrical and Computer Engineering, University of California Santa Barbara, Santa Barbara, CA 93106
hwchen@ece.ucsb.edu

Abstract: We demonstrate a phase modulator based on carrier depletion on the hybrid silicon evanescent platform. The device has a modulation efficiency of 4V/mm, along with a bandwidth of 100nm and power capability up to 20mW.

©2007 Optical Society of America

OCIS codes: (250.4410) Modulators; (250.5300) Photonic integrated circuits; (250.7360) Waveguide modulators.

1. Introduction

Silicon-based modulators have been successfully demonstrated by using carrier depletion in Mach-Zehnder interferometer (MZI) and ring resonator structures [1,2]. Conventional III-V semiconductor phase modulators utilizing quantum-confined Stark effect (QCSE) exhibit high modulation efficiencies but also large wavelength dependence. In order to minimize this wavelength dependence while maintaining modulation efficiency, phase modulators based on the carrier depletion effect in multiple-quantum-wells (MQW) have been demonstrated [3]. In this paper, we present a MQW MZI phase modulator on the hybrid silicon evanescent platform [4]. Our efficient carrier depletion modulators can be integrated as phase modulators or switches with lasers, amplifiers and photodetectors on silicon to make compact optical interconnects.

2. Device design and fabrication

The silicon evanescent phase modulator, as illustrated in Fig.1(a), is a hybrid structure consisting of III-V MQW bonded to a silicon waveguide fabricated on a silicon-on-insulator (SOI) wafer. The III-V epitaxial layers are shown in Table.1. Both the top separate confinement heterostructure (SCH) layer and MQW are doped in order to introduce free carriers. The thickness and doping of the top SCH layer is designed so as to be completely depleted in the absence of an externally applied electric field. Thus, all applied bias voltage will be used to deplete carriers in MQW region rather than SCH layer. The composition of wells and barriers are chosen to have shallower ΔE_c compared to electroabsorption modulators (EAM) and lasers in order to efficiently deplete the carriers. As shown in Fig. 2, the cladding width is 4 μm while the QW and SCH layers are under-cut to 2.8 μm to reduce the device capacitance. Silicon waveguides were fabricated with a waveguide height of 0.48 μm and slab height of 0.24 μm . The width of the waveguide is 1 μm and 1.5 μm in modulation and passive region respectively. Due to mode mismatch between these two sections, a 60 μm taper is added to minimize reflection and increase coupling efficiency. A 1x2 MMI, 6 μm wide and 40 μm long at the input, is used to split incoming light into the two arms of the MZI. For high speed performance, a microstrip line design is applied to the electrode as shown in Fig.1(b).

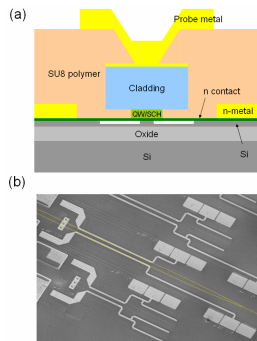


Fig. 1. (a) Schematic cross section of the hybrid waveguide (b) SEM overview of the device.

Layer	Material and Composition	Doping	Thickness	
1	Contact	$\text{In}_{0.53}\text{Ga}_{0.47}\text{As}$	$\text{P} - 1\text{e}19$	0.1 μm
2	Cladding	InP	$\text{P} - 1\text{e}18$	1.5 μm
3	SCH	$\text{In}_{0.53}\text{Al}_{0.165}\text{Ga}_{0.305}\text{As}$, 1.3 μm	$\text{N} - 1\text{e}17$	0.1 μm
4	QW ($\lambda_{\text{PL}} = 1.36 \mu\text{m}$)	$\text{In}_{0.574}\text{Al}_{0.111}\text{Ga}_{0.315}\text{As}$, +0.3%, 1.46 μm (15x)	$\text{N} - 1\text{e}17$	8 nm
		$\text{In}_{0.468}\text{Al}_{0.217}\text{Ga}_{0.315}\text{As}$, -0.41%, 1.16 μm (16x)	$\text{N} - 1\text{e}17$	5 nm
5	SCH	$\text{In}_{0.53}\text{Al}_{0.165}\text{Ga}_{0.305}\text{As}$, 1.3 μm	$\text{N} - 3\text{e}18$	0.05 μm
6	Contact	InP	$\text{N} - 3\text{e}18$	0.11 μm
7	Super lattice	$\text{In}_{0.85}\text{Ga}_{0.15}\text{As}_{0.327}\text{P}_{0.673}$ (2x)	$\text{N} - 3\text{e}18$	7.5 nm
		InP (2x)	$\text{N} - 3\text{e}18$	7.5 nm
8	Bonding	InP	$\text{N} - 3\text{e}18$	10 nm

Table 1. III-V epitaxial layer structure.

A standard process for fabricating silicon evanescent devices is used [4]. After wafer bonding, the mesa structure is fabricated using a self-aligned dry etch process [5] with Pd/Ti/Pd/Au p-contacts following by a wet etch to create the undercut. The sample is then dipped into a mixture of HCL/H₂O to remove native InO on the surface of the QW/SCH layers to avoid current leakage before depositing Ni/Au/Ge/Ni/Au n-contacts. A 4 μm thick polymer is used to provide additional mechanical support to the thin bonding layer and to separate the probe metal from the bottom n-metal in order to implement the desired microstrip line design and minimize parasitic capacitances.

3. Device characteristics

Fig.2 shows the modulation efficiency and extinction ratio (ER) at different wavelengths of a 1 mm long phase modulator. The experimental V_{π} is smaller at shorter wavelengths than at longer wavelengths because the QCSE is stronger at shorter wavelengths. A theoretical V_{π} curve based on band filling [7] and plasma effects at -2.5 V bias and 1 V swing is presented as well. The difference between theoretical values and experimental data at shorter wavelengths shows the existence of QCSE. The bandwidth is over 100 nm for ER greater than 10 dB. The ER is limited to 14 dB mainly due to the loss imbalance introduced by QCSE between the two arms of the MZI.

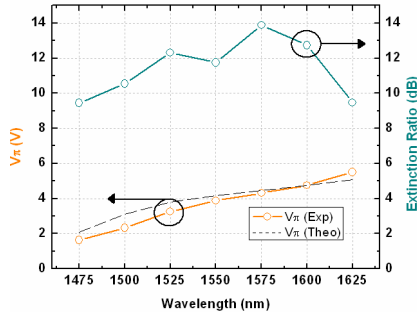


Fig. 2. V_{π} and extinction ratio at different wavelengths.

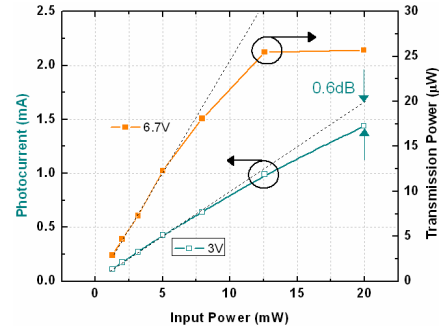


Fig. 3. Photocurrent and transmission power at -3 V bias at different input powers

To explore the possibility of high power operation, a 250 μm device was tested at 1550nm. Saturation dominated by the carrier screening effect is observed at -3 V bias with 20 mW input power as shown in Fig.3. Current breakdown is observed after -6.7 V bias with the same input power. Typical of the QCSE, the transmission power begins to saturate beyond 7.5mW input power with the bias maintained at -6.7 V.

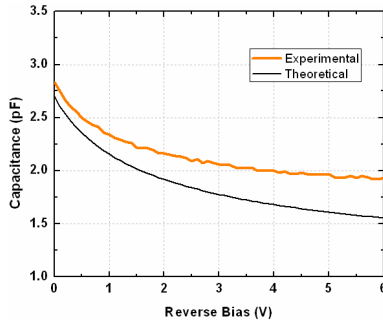


Fig. 4. Theoretical and measured CV for a 1 mm long device.

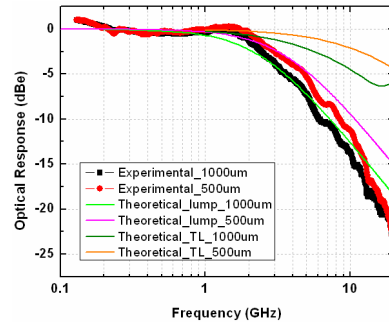


Fig. 5. Optical response at -3 V bias.

Two devices with 500 μm and 1000 μm were terminated by 50 Ω impedance and tested to determine high speed performance. In Fig.4, the experimental data starts to saturate earlier than theory suggests primarily because the doping concentration is not consistent over the MQW layer. Fig.5 shows the optical response of the device along with theoretical calculations of lumped and transmission line models. The response indicates that both devices are RC limited due to the 50 Ω termination. This can be improved by using a termination between 10 and 20 Ω .

4. Conclusion

A silicon evanescent MQW phase modulator capable of handling high optical powers and having broad optical bandwidth and efficient modulation is demonstrated. Extinction ratios greater than 10 dB between 1500 nm and 1600 nm allow application in WDM optical networks. The modulator exhibits $V_{\pi}L$ around 4 Vmm at 1550 nm and below 6 Vmm within a 100 nm range. Further, it is capable of handling optical powers up to 20 mW.

The authors acknowledge financial support from DARPA and the Army through contract W911NF-05-1-0175. The authors thank Matt Sysak, Alex Fang, Hyundai Park and Di Liang for useful discussions.

5. References

- [1] A. Liu, et al., "High-speed optical modulation based on carrier depletion in a silicon waveguide," *Opt Express* **15**, 660-668(2007).
- [2] Q. Xu, B. Schmidt, S. Pradhan, and M. Lipson, "Micrometre-scale silicon electrooptic modulator," *Nature* **435**, 325-327 (2005).
- [3] H. Ohe, et al., "InGaAlAs Multiple-Quantum-Well Optical Phase Modulators Based on Carrier Depletion," *IEEE Photon. Techno. Lett* **19**, 1816--1818 (2007).
- [4] A. W. Fang, et al., "Electrically pumped hybrid AlGaInAs-silicon evanescent laser," *Opt. Express* **14**, 9203-9210 (2006).
- [5] H. Park, et al., "A hybrid AlGaInAs-silicon evanescent preamplifier and photodetector," *Opt. Express* **15**, Issue 21, 13539-13546 (2007).
- [6] J. Vinchant, et al., "InP/GaInAsP guided-wave phase modulators based on carrier-induced effects: Theory and experiment," *IEEE J. Lightwave Techno.* **10**, 63-70 (1992).